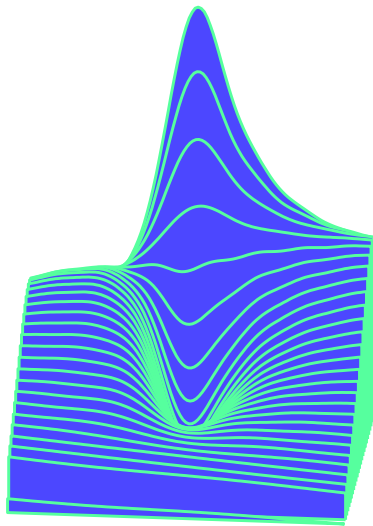


# Wave packet theory of resonant X-ray scattering

Paweł Sałek



KTH

Royal Institute of Technology  
Stockholm, 2001



## Abstract

This thesis presents time-dependent wave packet theory for resonant X-ray scattering (RXS) and applications of this theory to small molecules in the gaseous phase. The emphasis is put on aspects related to the dynamics of nuclear motion during the scattering process. The theory has been implemented in a new computer program which has been used in most of the investigations presented in the thesis.

The first part of the thesis addresses dissociative resonant photoemission from first principles. Particular emphasis is devoted to the conditions for observing so-called “atomic peaks” and “atomic holes”. The atomic peaks are connected with photoemission following resonant excitation to dissociative core excited states which show specific spectral bands from decay channels involving the dissociation fragments in addition to those involving the compound molecule.

The atomic holes are the results of continuum-continuum interference effects between these two, atomic and molecular, channels which may act destructively under certain conditions. We apply a novel electronic structure method to compute the transition moments for the resonant and direct photoemission channels including their dependence on internuclear distances and their interference. The prediction, and the subsequent confirmation, of the atomic holes, is an important result of this thesis. We demonstrate that the resonant contribution and the evolution of the atomic peaks can be subject to strong dynamical suppression caused by nuclear motion, so strong in fact that main state photoionization may constitute the dominating channel even at resonant conditions.

A Doppler effect for resonant X-ray scattering is predicted and verified. The physical grounds for this effect are presented. The radiative selection of the motion direction of the emitting atom with respect to the spectrometer gives rise to a Doppler shift of the Auger electron energy and results in a Doppler splitting of the atomic peak. We showed that a view of the Doppler effect as related with the phase of the emitted Auger electron leads to a generalization of ordinary Franck-Condon factors. The influence of such generalized factors was explored – and found consequential – for photoelectron spectrometry and for resonant non-radiative X-ray scattering experiments.

We discovered that the molecular geometry dependence of the electronic transition moments can change the RXS cross section quite dramatically; for instance, it was found responsible for an unusual spectral flattening for the B state of  $N_2$ , and for the breakdown of the spectator versus participator classification in a part of the non-radiative resonant photoemission spectrum of HF.

The notion of duration time in resonant X-ray scattering is presented in the first paper of the thesis; it was found to be a powerful concept for predicting and understanding qualitative aspects of many of the effects or processes treated in the following parts of the thesis. The role of the pulse shape for short pulse X-ray excitation is also studied.



# Preface

The usage of synchrotron radiation sources has become fairly common in the last years. These sources allow to irradiate samples in a broad energy region with light of high intensity and open an opportunity to perform a broad range of new experiments.

The development on the experimental side induces also a need for new theory that explains the details of the interaction between electromagnetic radiation and matter. Such theory has been developed in our division and I had a chance to join the effort to push forward the theory in some selected directions.

I focused on soft X-ray Raman scattering (150-700eV) on simple molecules in gaseous form. This includes many non-trivial cases that are on one hand interesting and on the other not overwhelmingly complex.

The research started from mostly analytical models, investigating general features of the RXS spectra, and gradually included more numerical ab initio methods to make our models applicable to the real experiment.

We were able to apply high accuracy methods for the calculations of the electronic structure of such molecules as well as develop and apply quantum wave packet methods that gave an insight into nuclear motion induced by the interaction with light.

The studies were performed in connection with our collaborators in Uppsala and at the Swedish synchrotron facility MAXLAB in Lund. This close collaboration yielded results and predictions where the development in the theory interleaved with new advances in the experimental field.

## List of papers

1. Duration of X-ray Raman scattering. F. Gel'mukhanov, P. Salek, T. Privalov and H. Ågren. *Phys. Rev. A* **59** No. 1, 380-389 (1999).
2. Wave packet dynamics of resonant X-ray Raman scattering: excitation near the Cl  $L_{II,III}$  edge of HCl. P. Salek, F. Gel'mukhanov and H. Ågren. *Phys. Rev. A* **59** No. 2, 1147-1159 (1999).
3. Observation of a continuum-continuum interference in ultrafast dissociating core-excited molecules. R. Feifel, F. Burmeister, P. Salek, M. N. Piancastelli, M. Bäbler, S. L. Sorensen, C. Miron, H. Wang, I. Hjelte, O. Björneholm, A. Naves de Brito, F. Kh. Gel'mukhanov, H. Ågren and S. Svensson. *Phys. Rev. Letters*, 85, 3133 (2000).
4. Dynamical suppression of atomic peaks in resonant dissociative photoemission. P. Salek, V. Carravetta, F. Kh. Gel'mukhanov, H. Ågren, B. Schimmelpfennig, M. -N. Piancastelli, S. L. Sorensen, R. Feifel, I. Hjelte, M. Bässler, S. Svensson O. Björneholm, and A. Naves de Brito. Submitted.
5. Theory and first principle calculations of dissociative resonant photoionization. The evolution of atomic peaks and holes. P. Salek, V. Carravetta, F. Gel'mukhanov and H. Ågren. Submitted.
6. Numerical implementation of a wave packet techniques in X-ray scattering P. Salek. In manuscript.
7. X-ray Raman scattering under pulsed excitation. F. Gel'mukhanov, P. Salek, A. Shalagin, and H. Ågren. *J. Chem. Phys.* **112**, No 13, 5593-5603 (2000).
8. Doppler effects in X-ray Raman scattering. F. Gel'mukhanov, H. Ågren, and P. Salek. *Phys. Rev. A* **57**, No 4, 2511-2526 (1998).
9. Generalized Frank-Condon principle for resonant photoemission. P. Salek, F. Gel'mukhanov, H. Ågren, O. Björneholm and Svante Svensson. *Phys. Rev A* **60** No. 4 2786-2791 (1999).
10. Doppler effect for bound nuclear motion and its manifestation in resonant photoemission of oriented systems. P. Salek, F. Gel'mukhanov, T. Privalov and H. Ågren. *Chem. Phys. Lett.*, 328, 425 (2000).

- 
11. Vibrationally resolved core photoelectron spectroscopy as an  $\infty$ -slit interferometry. F. Gel'mukhanov, P. Salek and Hans Ågren. Accepted in Phys. Rev. A.
  12. Resonant X-ray Raman scattering involving avoided crossings in the final state potential energy curves. P. Salek, R.F. Fink, F. Gel'mukhanov, M.N. Piancastelli, R. Feifel, M. Bäßler, S. L. Sorensen, C. Miron, H. Wang, I. Hjelte, O. Björneholm, A. Ausmees, S. Svensson, and H. Ågren. Phys. Rev. A, 62, 062506 (2000).
  13. Competition between decay and dissociation of core-excited carbonyl sulfide studied by X-ray scattering. M. Magnusson, J. Guo, C. Sâthe, J.-E. Rubensson, J. Nordgren, P. Glans, L. Yang, P. Salek and H. Ågren. Phys. Rev. A **59** No. 6, 4281-4287 (1999).
  14. Picturing molecular femtosecond processes through an ultrafast controllable X-ray shutter. H. Ågren, F. Gel'mukhanov, P. Salek, S. Svensson and J. Nordgren. In manuscript.
  15. Dynamics of Inner Shell Resonant Raman Scattering. H. Ågren, F. Gel'mukhanov, and P. Salek. J. of the Jap. Society for Synchrotron Radiation Research, **12**, No 4, 257-267 (1999).

## Acknowledgements

This thesis is based on research begun in the Computational Physics Division at Linköping University, continued and finished in the Theoretical Chemistry Division at the Royal Institute of Technology. I acknowledge Professor Hans Ågren for his guidance during all these years. Also, Prof. Faris Gel'mukhanov is gratefully acknowledged: The studies under his command have been very rewarding and fruitful.

I acknowledge all other senior researchers in our group. In particular, I thank Dr. Bernd Schimmelpfenning for his help on scientific field, patience, companionship and... being less stingy that I am sure he could be. ☺

I thank Prof. Vincenzo Carravetta for fruitful collaboration on resonant photoemission. The collaboration with the experimentalists in Uppsala and at MAXLAB laboratory in Lund was very productive. I am very happy I had a chance to work with Raimund Feifel, Florian Burmeister, Stacey Sorensen, Margit Bäßler, Maria-Novella Piancastelli, Karoline Wiesner (long live Linux!), Svante Svensson and many others.

I would also like to thank all the PhD students in our division and particularly those who graduated in the group, in particular Patrick Norman, Dan Jonsson and Oles Plashkevych: They have been exemplary PhD students. I was intimidated by their research and thick theses with numerous articles published in world-class journals and kept telling myself that the size of the thesis does not matter. I tried to take my revenge on the innebandy playfield but it was difficult to compete with guys born with bandy sticks in their hands. I tried to do my best anyway. I should mention here also Peter Cronstrand and Maria Engström who so willingly suffered talking Swedish with me.

I feel gratitude to all anonymous people I met in my life, everyone that shared with me their time. Thanks for being there for me.

Last but not least, I would like to thank Dorota for her patience and support... and everything else.

Thanks.

Paweł Sałek,                      Stockholm, May 2001

# Contents

<b>1</b>	<b>Resonant X-ray scattering</b>	<b>1</b>
1.1	The experiment . . . . .	1
1.2	Raman law . . . . .	4
1.3	Scattering duration . . . . .	6
1.4	Characteristic time of nuclear motion . . . . .	7
<b>2</b>	<b>Time-dependent RXS theory</b>	<b>9</b>
2.1	Time dependent formalism . . . . .	10
2.2	Transition moments. Light polarization . . . . .	11
2.3	Doppler correction to X-ray scattering . . . . .	12
2.4	Generalized Franck-Condon factors . . . . .	15
2.5	RXS under core excitation to dissociative states . . . . .	16
2.6	HF – the merge of electronic and vibrational theories . . . . .	20
<b>3</b>	<b>Wave packet methods</b>	<b>25</b>
3.1	Absorption calculations . . . . .	26
3.2	Time-dependent techniques . . . . .	27
<b>4</b>	<b>Molecular electronic structure</b>	<b>31</b>
4.1	Potential surfaces . . . . .	32
4.1.1	HF method . . . . .	33
4.1.2	MCSCF method . . . . .	34
4.1.3	Other high accuracy methods . . . . .	34
4.2	Computation of transition amplitudes . . . . .	35
	<b>Summary</b>	<b>39</b>



# Chapter 1

## Resonant X-ray scattering

### 1.1 The experiment

Resonant X-ray Raman scattering (RXS) is a spectroscopic technique for studying the electronic structure of atoms and molecules as well as solid matter[1, 2, 3, 4, 5, 6, 7]. In an RXS experiment, the sample is irradiated with X-rays that are able to excite electrons occupying tightly-bound core orbitals. The core-excited states created in this way are short-lived – the lifetime is often of the order of few femtoseconds – and decay to one of many possible final states, which usually are valence excited states. From the electronic structure point of view, there exists two distinct decay channels: *radiative* – when another X-ray photon is emitted, or *non-radiative* – when the extra energy is released through Auger electron emission.

In this thesis, we develop, implement and apply theory describing X-ray Raman scattering on free molecules. Because of low matter density, the experiment requires light of high intensity and is usually performed using synchrotron facilities. The schematic experimental setup is shown on Figure 1.1. The synchrotron ring is a source of fast electrons having energies in the GeV range. The electrons pass through a magnetic field where they decelerate and emit coherent electromagnetic radiation in a broad energy range from a few to thousands of eVs. The first synchrotron light sources (SLS) used bending magnets to decelerate electrons. The second generation SLSes introduced in the 70-ies used wigglers as the light generation elements. Currently, most of the used SLSes belong to the so-called third generation and generate light using undulators. The generated

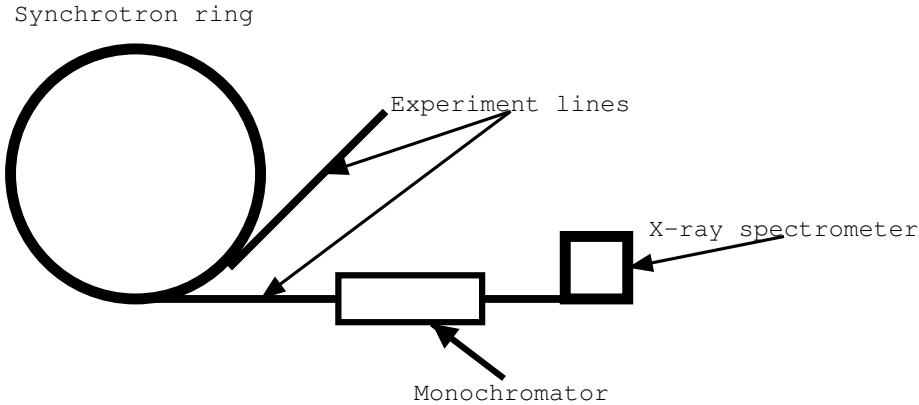


**Fig. 1.1:** The scheme of RXS experiment performed using synchrotron X-ray source.

photon flux is of the order  $10^{11} - 10^{12} \text{ s}^{-1}$ . There is ongoing work to create fourth generation light sources – so-called free electron lasers – which produce light of even higher intensity by spontaneous emission from free electrons.

The light emitted by the retarding electrons passes through a set of focusing and monochromatizing equipment and hits the sample. The scattered photons or electrons are then collected by a spectrometer. The branching ratio between radiative and nonradiative decay depends on the Z-number of the excited atom and is schematically illustrated on Figure 1.2. While the scattering process is founded on the same principles for radiative and non-radiative scattering, spectrometers collecting Auger electrons have higher efficiency than photon spectrometers, which give better statistics in non-radiative experiments.

The irradiated gas interacts with the radiation field through the dipole moment  $\mathbf{D}$  of the molecule as given by the absorption cross section

$$\sigma \sim |\langle \Phi_c | \mathbf{D} \cdot \mathbf{e} | \Phi_0 \rangle|^2, \quad (1.1)$$

where  $\mathbf{e}$  is the X-ray photon polarization vector. The X-ray photons have sufficient energy to excite the core electrons to an unoccupied orbital or even to ionize the molecule. The RXS process occurs when the photon energy  $\omega$  is chosen below the core electron ionization threshold. The created core-excited state subsequently decays emitting excessive energy with a photon or an Auger electron of energy  $E$  that can later be measured by an energy-dispersive spectrometer. The energy released in the decay process can be estimated from the energy con-

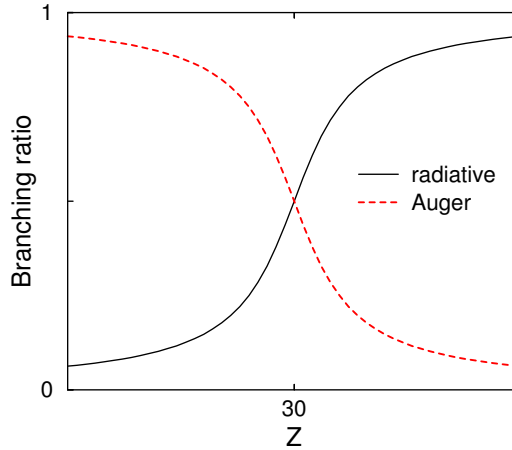


**Fig. 1.2:** Illustration of the dependence of radiative vs non-radiative branching ratio (relative decay rates) in X-ray scattering on  $Z$  atomic number.

servation law – it is important though to take the vibrational energy into account since the molecule in the core-excited state can enter a vibrationally excited state or even dissociate as depicted on Figure 1.3. The excitation energy is transferred to vibrational degrees of freedom and the released energy will change.

The excitation and decay processes happen so quickly relative to the nuclear vibration speed that one can say that the electronic wave functions (and associated potentials surfaces) switch suddenly without any change of the nuclear wave function. The *Franck-Condon (FC) principle* states that an electronic transition takes place so rapidly that a vibrating molecule does not change its geometry appreciably during the transition. In other words, the transition is *vertical* from the nuclear point of view; the molecular energy changes but not the internuclear distance. The related Frank-Condon amplitude is defined as an overlap  $\langle \phi | k \rangle$  between an arbitrary nuclear state  $|\phi\rangle$  and an eigenstate  $|k\rangle$  of the nuclear Hamiltonian. It defines a probability distribution between vibrational – or continuous – modes after the transition. This overlap between nuclear states appears in this or a similar form in many places of the RXS theory.

The interplay between the vibrational motion and decay process opens an entire new field of investigations, which also is the subject of this thesis. One can observe that for fast decay processes, the wave packet on the core-excited potential surface will not have time to evolve – and the scattering spectrum will

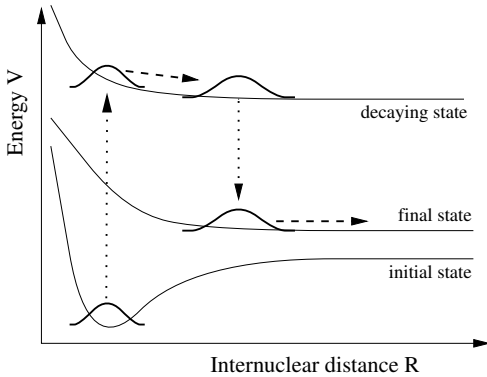


**Fig. 1.3:** The general principle of Raman scattering. The molecule is excited from the initial state  $|0\rangle$  to the intermediate state  $|c\rangle$  and decays after some time to the final state  $|f\rangle$ .

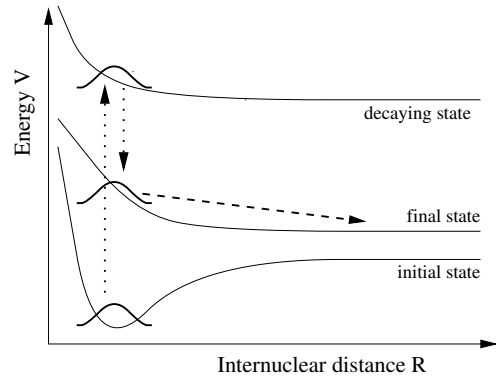


**Fig. 1.4:** The principle of Raman scattering through the decaying state  $|c\rangle$  of short lifetime. Since the lifetime of  $|c\rangle$  is very short, the initial wave packet appears on the final surface unchanged.

be similar to the one of the absorption directly to the final state as seen on Figure 1.4. The other limiting case is when the core-hole state is long-lived and the molecule dissociates before the decay. The decay process will be analogous to the one occurring in single atoms and the spectrum will consist of narrow atomic peaks at positions determined by the energy differences between atomic energy levels. The intermediate case when the core-hole state  $\Phi_c$  has a lifetime  $\Gamma^{-1}$  of the same order as the dissociation time leads to a cross section simultaneously having a molecular background as well as atomic peaks. These fast and slow decay channels will interfere giving rise to rich spectra providing much information about the scattering process.

## 1.2 Raman law

Let us start from the simplified Kramers-Heisenberg formula describing the X-ray Raman scattering cross section in order to find out basic properties of the cross section and its dependence on the photon frequency  $\omega$ . We focus on the resonant contribution to the cross section only and neglect any geometry dependence of the electronic transition moments and their absolute value. We obtain the following expression for the cross section  $\sigma(\omega, E)$  as a function of  $\omega$  and the emitted particle

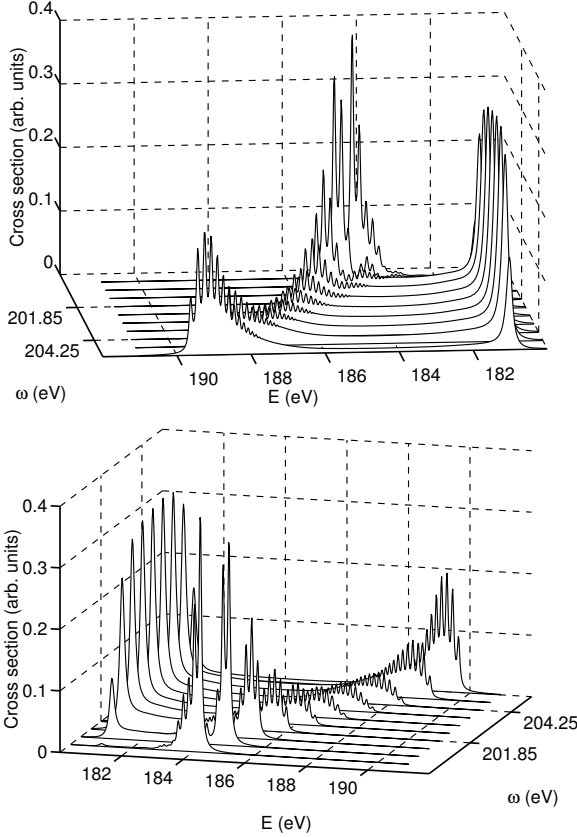


**Fig. 1.5:** The RXS cross section  $\sigma(\omega, E)$  for  $2p$  core-excited HCl molecule and lowest  ${}^2\Sigma^+$  final state. The molecular part corresponding to the fast decay moves according to the Raman law while the atomic peak remains at the same position. See paper 2.

energy  $E$

$$\sigma(\omega, E) \sim \sum_f \left| \sum_c \frac{\langle f|c\rangle\langle c|0\rangle}{\omega - (E_c - E_0) + i\Gamma} \right|^2 \delta(E + E_f - E_0 - \omega). \quad (1.2)$$

Here,  $|0\rangle$ ,  $|c\rangle$  and  $|f\rangle$  are vibrational wave functions of ground, core-excited and final states, respectively, and  $E_0$ ,  $E_c$  and  $E_f$  are associated energies. The cross section is expressed through the sum over all final states  $|f\rangle$ . Since the numerator is energy independent, the magnitude of the cross section as function of photon energy  $\omega$  is determined by the denominator. This denominator blows up for a photon energy equal to one of the resonance frequencies  $\omega = E_c - E_0$ . An interesting experiment that can be performed is to investigate the cross section evolution on the detuning from the resonance.

Also, we learn from Eq. (1.2) that the dependence of the final particle (photon or Auger electron) energy,  $E$ , on the excitation energy is determined by the  $\delta$  function and is

$$E = \omega - (E_f - E_0) . \quad (1.3)$$

This is the so-called Raman law. Figure 1.5 shows the RXS cross section computed for the HCl molecule; it can be clearly seen that the molecular part behaves according to the Raman law with detuning while the position of the atomic peak remains constant.

### 1.3 Scattering duration

We would like to emphasize another feature of RXS and consider the Kramers-Heisenberg formula (1.2) in the case of large detuning  $\Omega = \omega - (E_c - E_0)$ , or large lifetime broadening,  $\sqrt{\Omega^2 + \Gamma^2} \gg \omega_{\text{vib}}$ , where  $\omega_{\text{vib}}$  is the vibrational frequency. The closure condition

$$\sum_c |c\rangle\langle c| = 1 \quad (1.4)$$

results immediately in

$$\sigma(\omega, E) \sim \sum_f |\langle f|0\rangle|^2 \delta(E + E_f - E_0 - \omega) \quad (1.5)$$

This equation has a very interesting interpretation. We received that in the case of the period of vibrations  $\tau_{\text{vib}} = 2\pi/\omega_{\text{vib}}$  being shorter than  $(\Gamma^2 + \Omega^2)^{-1/2}$ , the RXS process is fast and corresponds to a sudden transition to the final state  $|f\rangle$  since the nuclear wave packet has no time to evolve on the core-excited potential surface. This allows us to interpret

$$T = \frac{1}{\sqrt{\Gamma^2 + \Omega^2}} \quad (1.6)$$

as the RXS duration time.

Also, we have used the completeness of the intermediate vibrational states (1.4) in order to derive the limiting case (1.5). This means that the RXS duration time is essentially a quantum notion and closely related with the state interference – see paper 2.

The concept of RXS duration time appears frequently in the RXS theory. It is also quite appealing from the experimental point of view by providing means to

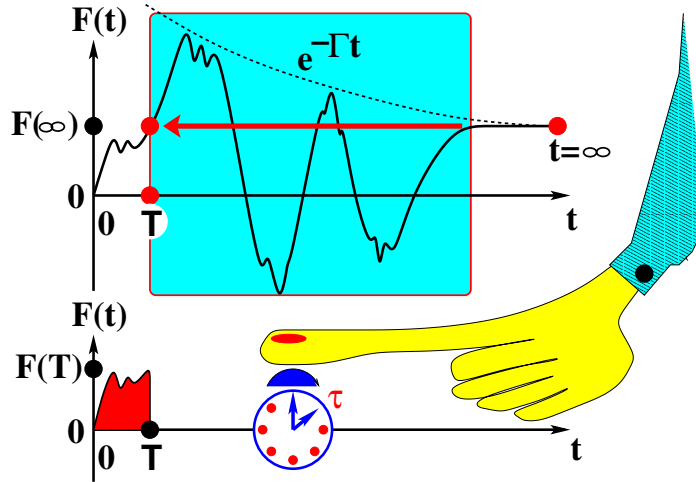


**Fig. 1.6:** The detuning as means of controlling the duration of the scattering process,  $T$ . Only short-time contributions form the RXS amplitude,  $F$ , because of the destructive interference for larger times  $t$ .

control the scattering time: While the core-excited state lifetime is a molecular property, the incident photon frequency can be chosen at will. We see that the timing for the scattering process is possible via the frequency detuning of RXS, which acts effectively as a camera shutter analogous to time dependent pump-probe measurements, Fig. 1.6.

## 1.4 Characteristic time of nuclear motion

The other characteristic time apart from the scattering time is the one that characterizes the motion of the wave packet. For a bound state, the vibration period can be estimated as

$$\tau_{\text{nucl}} \simeq \frac{1}{\Delta_{\text{vib}}}$$

For ordinary diatomic molecules, the distance between vibrational levels is of the order 0.1 – 0.3 eV and the period of the vibrational motion is about 15 – 20 fs.

The character of the decay is different if the scattering time  $T$  is shorter than the vibration time; the core-excited state decays before the molecule manages to

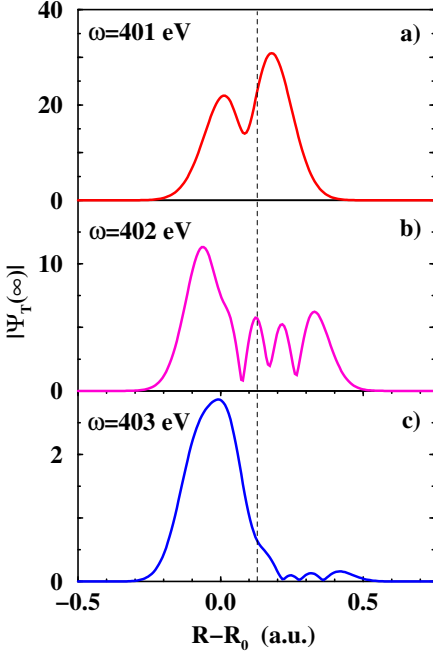


**Fig. 1.7:** The space distribution of  $|\Psi_T(\infty)|$  versus the RXS duration (detuning) for the bound core-excited state  ${}^1\Pi_u$  of  $\text{N}_2$ . The contribution of the region outside of the ground state vibrational wave function is suppressed when  $\Omega$  is large. The RXS duration times are:  $|T| \simeq 5.6$  fs, 0.73 fs, and 0.35 fs for the excitation frequencies  $\omega = 401$  eV (at resonance), 402 eV, and 403 eV, respectively. See paper 1.

perform one entire vibration. The vibrational structure of the core-excited state cannot be seen anymore.

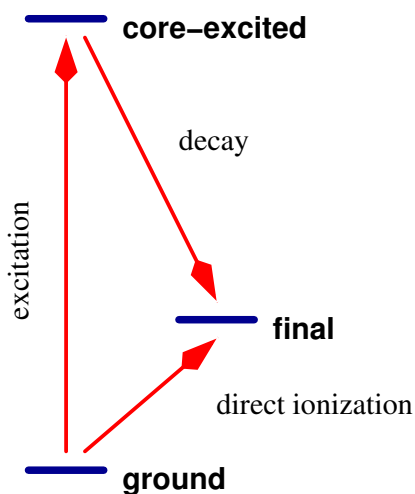
The characteristic time  $\tau_{\text{nucl}}$  in the case of dissociative core excitation is the dissociation time. Again, if the molecule dissociates faster than it decays, the RXS spectrum will look like a spectrum of a core-excited atom. In the opposite limit of fast decay, the spectrum will be more direct photoionization alike.

Figure 1.7 shows that the spectral shape of RXS depends strongly on the interplay of the RXS duration and characteristic time of the wave packet evolution  $\tau_{\text{nucl}}$ . The RXS duration gives us a tool of an active operation by the physical processes with the different time scales which influence the RXS profile. When the duration  $T$  is small (large  $\Omega$ ) the nuclear wave packet has no time to evolve in the core-excited potential surface and copies the narrow ground state nuclear wave function (see Fig. 1.7c).

## Chapter 2

# Time-dependent RXS theory

The fundamental theory of X-ray Raman scattering has been developed in the seventies of the previous century but the interest in this field of physics was initially rather limited until the rapid development of the high intensity synchrotron light sources made it possible to verify theoretical predictions. Many new and fundamental features have been revealed in the spectra and some of them – explained. Below, an abridged survey of the research contained in the included articles is presented.



**Fig. 2.1:** Simplified scheme of RXS. The electronic energy levels are assumed to be constant under scattering. Two channels are allowed: either Raman scattering with an emission of an Auger electron, or direct photoionization. Because the final states are identical, these two channels will interfere.

## 2.1 Time dependent formalism

It is now well established that both radiative and nonradiative RXS can be described on the same footing making use of the Kramers-Heisenberg formula. The extended – including direct photoionization channel – Kramers-Heisenberg formula describing the scattering cross section connected with emission of a particle of energy  $E$  is

$$\sigma(\omega, E) = \sum_f \left| \langle f | \hat{Z} | 0 \rangle + \sum_c \frac{\langle f | \hat{Q} | c \rangle \langle c | \hat{V} | 0 \rangle}{E - E_c + E_f + i\Gamma} \right|^2 \Phi(E + E_f - \omega - E_0, \gamma) \quad (2.1)$$

where the emitted particle can be either a photon in the case of radiative decay, or an Auger electron in the case of non-radiative decay, and where  $\Phi(\omega, \gamma)$  is the spectral function of the incident radiation with the spectral width  $\gamma$ . The excitation operator  $\hat{V}$  is an ordinary dipole moment operator between the ground electronic and the core-excited states. The decay operator  $\hat{Q}$  is a dipole moment operator between core-excited and final states in the case of radiative decay, or a Coulomb operator in the case of non-radiative scattering. We include also in the formalism the direct photo-ionization term associated with the dipole transition operator  $\hat{Z}$  between ground and final electronic states. The transition operators can be factored out when one is interested in the spectral shape of the cross section only – assuming that these operators do not strongly depend on the molecular geometry which is often the case. The molecular geometry dependence of the excitation operators  $\hat{Z}$  and  $\hat{V}$  is practically always negligible because the right-hand state  $|0\rangle$  being the ground state wave packet is well localized in space. On the other hand, the core-excited  $|c\rangle$  and final  $|f\rangle$  wave packets are often delocalized and there exist some cases where the geometry dependence of the decay operator  $\hat{Q}$  is the key point in the explanation of the RXS spectrum – see for example paper 12 in this thesis. The lifetime  $\Gamma^{-1}$  of the core-excited state determines not only the width of the absorption band, but being connected to the core-excited state total decay rate, it changes also the spectral shape of the scattering spectra.

The Kramers-Heisenberg formula can be rewritten to the time-dependent formalism yielding

$$\sigma(\omega, E) = \int \sigma_0(\omega', E) \Phi(\omega - \omega', E) d\omega' \quad (2.2)$$

$$\sigma_0(\omega, E) = \frac{1}{\pi} \text{Re} \int_0^\infty \sigma(\omega, \tau) e^{i(\omega - E)\tau} d\tau \quad (2.3)$$

$$\begin{aligned} \sigma(\omega, \tau) = & \langle \Psi(0) | e^{-i(\hat{H}_f - E_0)\tau} | \Psi(0) \rangle + \langle 0 | \hat{Z}^\dagger e^{-i(\hat{H}_f - E_0)\tau} \hat{Z} | 0 \rangle \\ & + i \{ \langle \Psi(0) | e^{-i(\hat{H}_f - E_0)\tau} \hat{Z} | 0 \rangle - \langle 0 | \hat{Z}^\dagger e^{-i(\hat{H}_f - E_0)\tau} | \Psi(0) \rangle \} \end{aligned} \quad (2.4)$$

where  $|\Psi(0)\rangle$  expresses a wave packet integrated over its entire evolution time on the core-excited potential surface and containing the entire non-trivial dependence of the cross section on detuning

$$|\Psi(0)\rangle = \hat{Q} \int_0^\infty e^{-i(\hat{H}_c - E_0 - \omega)t} \hat{V} | 0 \rangle e^{-\Gamma t} dt \quad (2.5)$$

$$|\Psi(\tau)\rangle = e^{-iH_f\tau} |\Psi(0)\rangle \quad (2.6)$$

The correlation function in (2.4) has three major terms. The first one expresses the resonant cross section, the second one – the photoionization channel, and the third one is the interference term between the resonant and direct channels.

Equation (2.4) is different for a homonuclear molecule because the wave functions of emitted electrons from two atoms differ by a phase factor. The correlation function then becomes

$$\sigma_0(\tau) = \sigma_0^{(1)}(\tau) + \sigma_0^{(2)}(\tau) + \sigma_0^{(12)}(\tau) \quad (2.7)$$

$$\sigma_0^{(j)}(\tau) = \langle \Psi^{(j)}(0) | \Psi^{(j)}(\tau) \rangle \quad j = 1, 2 \quad (2.8)$$

$$\sigma_0^{(12)}(\tau) = \langle \Psi^{(1)}(0) | \Psi^{(2)}(\tau) \rangle + \langle \Psi^{(2)}(0) | \Psi^{(1)}(\tau) \rangle \quad (2.9)$$

where the difference between  $|\Psi^{(1)}(\tau)\rangle$  and  $|\Psi^{(2)}(\tau)\rangle$  is in the  $\hat{Q}$  operator:

$$\hat{Q}_1 = \hat{Q}_0 e^{-i\alpha\mathbf{k}\cdot\mathbf{R}} \quad \hat{Q}_2 = \hat{Q}_0 e^{+i\alpha\mathbf{k}\cdot\mathbf{R}}. \quad (2.10)$$

(the direct and corresponding interference terms are neglected for simplicity). Here,  $\mathbf{k}$  is the momentum of the emitted Auger electron,  $\alpha = m_B/(m_A + m_B)$  is the mass ratio coefficient equal to  $\frac{1}{2}$  for a homonuclear molecule and  $\mathbf{R}$  is the radius vector. The three terms in Eq. (2.7) correspond to the scattering cross section on the first atom, the second atom, and the interference between them, respectively.

## 2.2 Transition moments. Light polarization

We argued earlier that the transition moments can usually be factored out from the cross section expressions. We will discuss now the conditions when this trans-

formation can be carried out and what the consequences of the transformation are.

The transition moments  $\hat{Z}$ ,  $\hat{V}$  and  $\hat{Q}$  are molecular properties that can be deduced from the electronic structure of the investigated molecule. As such, they can change with the molecule geometry they are computed at. We explained earlier that this dependence can often be neglected for excitation transition moments  $\hat{Z}$  and  $\hat{V}$  because they operate on the ground state wave packet  $|0\rangle$  which is localized around the equilibrium geometry of the molecule and the transition moments being smooth functions of the geometry are unlikely to change rapidly in such a limited region.

Even in the case of weak geometry dependence, a calculation that includes both the resonance and direct photoionization terms needs the values of the transition moments to preserve the correct ratio between the two channels.

The decay transition moment  $\hat{Q}$  behaves differently; this operator is folded between core-excited and final states that are in principle extended over a much larger range of molecular geometries (particularly in the case of dissociative electronic states) and the geometry dependence of this parameter may have substantial influence on the cross section. A good example is the B-state of the core-excited  $N_2$  as plotted on Fig. 2.3: The original lifetime vibrational interference (LVI) formula[8, 9, 10, 11] cannot explain the unusual flattening of the spectrum. This effect occurs due to a strong  $R$ -dependence of transition moments for this state; the  $R$ -dependence can be attributed to an avoided crossing between “dark” and “bright” electronic configurations.

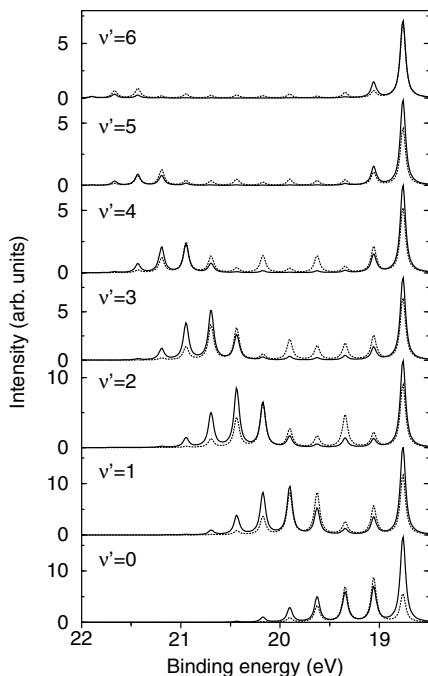
The other important quantity is the polarization  $\mathbf{e}$  of the incident light. It adds an orientation sensitive factor to the transition moment

$$\hat{V} = \mathbf{e} \cdot \mathbf{D}_{co} . \quad (2.11)$$

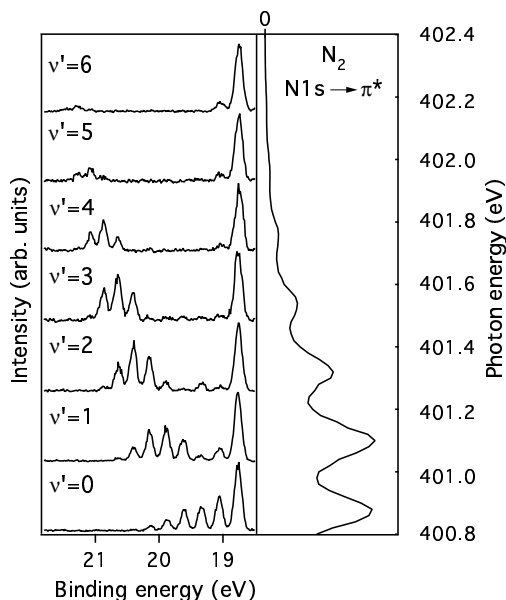
This equation shows that the incident photon excites molecules only with a certain orientation

$$\mathbf{D}_{co} \parallel \mathbf{e}$$

Such an oriented ensemble of core-excited molecules gives rise to an anisotropy of the emitted electrons and X-ray photons even for disordered samples[12, 13].



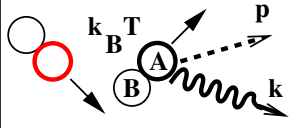
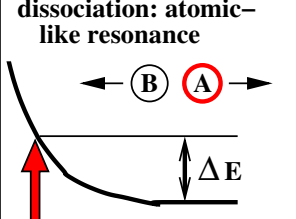
**Fig. 2.2:** Comparison of cross sections obtained for  $N_2$  from the strict LVI formula[8] and our formalism with  $R$ -dependent transition moments included. See paper 12.



**Fig. 2.3:** Experimental spectrum of the B state of  $N_2$ . See paper 12 for further details.

## 2.3 Doppler correction to X-ray scattering

There is another element in the scattering that has to be taken into account: The Auger electron is not emitted from a molecule at rest but from a dissociating one, or one in a vibrational motion – and the molecular center of mass is moving as well. Generally, there are more Doppler-type effects as classified on Figure 2.4, but only the Doppler effect associated with the electron emission in the dissociative motion can be measured with currently available apparatus. In the case of the electron Doppler effect, the value of the measured energy for the electron depends on the fact whether the emitting atom was approaching the detector (the measured energy will be then higher) or was moving away from it. The energy difference can

	Photon Doppler effect	Electron Doppler effect
<b>thermal motion</b> 	<b>Doppler</b> $\bar{v} = \sqrt{\frac{2k_B T}{M}}$ $p\bar{v} \sim 10^{-3} \text{ eV}$	<b>broadening</b> $k_B T = 0.03 \text{ eV}$ $k\bar{v} \sim 10^{-2} \text{ eV}$
<b>dissociation: atomic-like resonance</b> 	$v_A = \frac{\sqrt{2\mu \Delta E}}{m_A}$ $p v_A \sim 0.01-0.05 \text{ eV}$	$\Delta E \sim 1-10 \text{ eV}$ $k v_A \sim 0.1-0.5 \text{ eV}$

**Fig. 2.4:** Classification of Doppler effects. Four possible contributions to the Doppler shift are shown. The electron Doppler effect in the dissociative motion is the largest one and the only one measured so far.

be explained by an additional Doppler term included in the energy conservation equation

$$E = \omega + E_0 - E_f - \epsilon_f - (\mathbf{p} - \mathbf{k}) \cdot \mathbf{V} \quad (2.12)$$

where  $\mathbf{p}$  is the momentum of the incoming photon,  $\mathbf{k}$  is the Auger electron momentum and  $\mathbf{V}$  is the speed of the emitting atom with respect to the detector. The photon momentum  $\mathbf{p}$  is in the soft X-ray region and can therefore be neglected. This is though not the case for the electron momentum  $\mathbf{k}$ .

The simplest way to include Doppler effects into the RXS theory at a quantum level is through the so-called generalized Franck-Condon factors (GFC) introduced in paper 9. The speed of the emitting atom A in the molecule AB is effectively included in the phase factor of the decay operator  $\hat{Q}$  which then becomes explicitly dependent on the molecule geometry  $\mathbf{R}$  – see Eq. (2.10).

The Doppler effect is easiest to observe when the molecule dissociates in its core-excited state. The scheme of the experimental setup is shown on Figure 2.5. The core-excited molecules are aligned along the polarization vector  $\mathbf{e}$  under core excitation  $1s \rightarrow \sigma$  as described by Eq. (2.11). This results in two qualitatively dif-

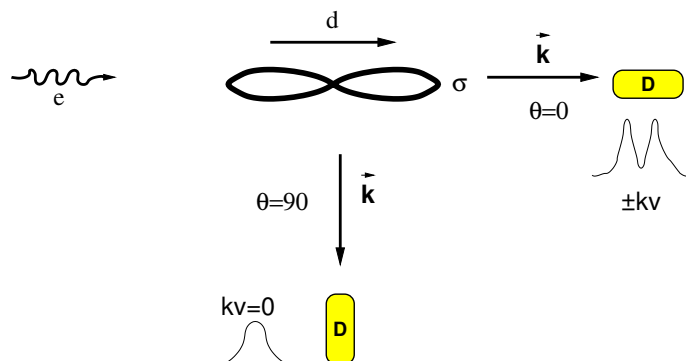


**Fig. 2.5:** Schematic illustration of the origin of the Doppler effect in RXS of a diatomic molecule.

ferent experimental geometries: a)  $\mathbf{e} \parallel \mathbf{k}$  – the emitted Auger electron has opposite Doppler shift for atoms approaching the detector or moving away ( $\theta = 0^\circ$ ). The Doppler splitting is observed; b)  $\mathbf{e} \perp \mathbf{k}$ . Now the Doppler shift is absent,  $\mathbf{k} \cdot \mathbf{v} = 0$  and only a single resonance is observed ( $\theta = 90^\circ$ ). Here,  $\theta$  is the angle between the incident photon polarization axis  $\mathbf{e}$  and the Auger electron momentum  $\mathbf{k}$ . The total spectrum is a result of averaging over all possible orientations of the dissociating molecule with the weight factor containing the nonisotropic excitation cross section.

It was shown in paper 10 that the Doppler effect can even be observed when the core-excited state is bound as long as the lifetime of the core-excited state is of the same order of magnitude as the period of vibrational motion. An example is given in Fig. 2.8: Although the potential of the core-excited state is bound, the wave packet decays only while moving outwards. The Doppler effect could not be observed if the lifetime of the core-excited state was much longer because the wave packet would move in both directions during the decay. The effect would not be observed if the lifetime was too short neither: The wave packet would not have time to move at all.

## 2.4 Generalized Franck-Condon factors

The generalized Franck-Condon factors enter not only in RXS theory but also influence spectra measured in photoelectron spectroscopy (PES) as explained in

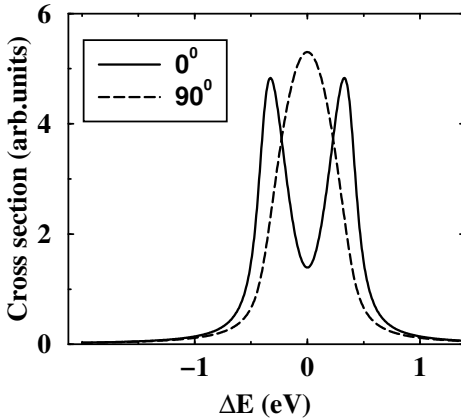


**Fig. 2.6:** The RXS profile for the isolated atomic-like resonance averaged over molecular orientations. Core excitation to the unoccupied  $\sigma$  orbital. The results of the simulations for  $\theta = 0^\circ$  and  $90^\circ$  are shown.  $\theta$  is the angle between  $\mathbf{k}$  and  $\mathbf{e}$ .  $\Gamma = 0.09$  eV. See paper 8.

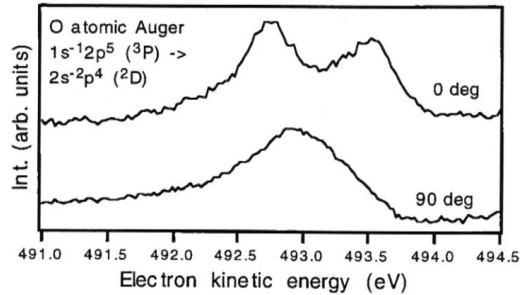


**Fig. 2.7:** The Doppler splitting of the atomic peak measured for the  $1s \rightarrow \sigma^*$  core-excited  $O_2$  molecule. The spectra were measured for two different angles between the X-ray photon polarization direction and the detection direction. From Ref. [14].

paper 11. The principle is illustrated in Figure 2.9. The electromagnetic field absorbed by the vibrating molecule has a different phase depending on the vibrational phase. The phase difference depends on the internuclear distance at the moment of absorption as well as on the photon wavelength. The interference between these coherent waves can considerably influence the vibrational profile of the core photoelectron spectra. The interference averages out to a large extent for free molecules but the effect can make a dramatic difference for surface physisorbed molecules: The computed cross sections demonstrating this effect for CO are shown in Figure 2.10.

## 2.5 RXS under core excitation to dissociative states

The RXS spectral profile has two major contributions which are formed by the decay transition in molecular and dissociative regions – see Fig. 2.11 [15].

The initially localized wave packet moves to the dissociative region and spreads. During this propagation the wave packet decays continuously to the final state.

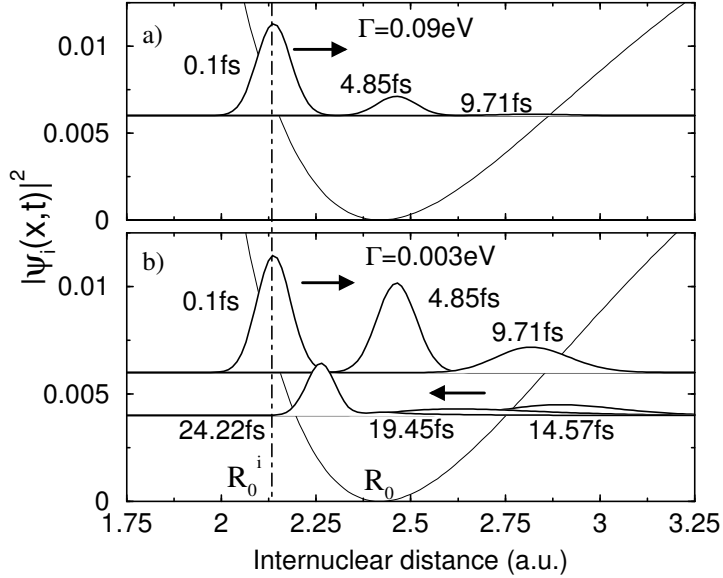


**Fig. 2.8:** Wave packet evolving on the core-excited potential surface of  $N_2$ . The upper plot shows wave packet evolution for a lifetime of the core-excited state of  $\Gamma = 90$  meV. This short lifetime causes the wave packet to decay completely during the first half of the period. See paper 10.

The decay processes near the equilibrium geometry form the so-called molecular band. When the wave packet approaches the region of dissociation, the decay is identical to the one of one of the fragments. This decay channel forms narrow *atomic*-like resonances when the dissociation fragment is just a single atom.

The scattering process depends strongly on the energy of the incident photon. The off-resonance excitation decreases the total magnitude of the cross section but the atomic features vanish faster than the molecular ones with detuning. The spectrum becomes similar to the direct photoionization cross section for large detuning. Detuning can then be treated as a parameter controlling dissociation in the core-excited state.

Since the atomic peak is localized at a constant position and the molecular background moves with changed detuning, these contributions to the cross section can overlap for a range of detuning parameters and the atomic-like resonance can be embedded in the molecular background. Such a case leads to an interference between the molecular and atomic decay channels since the final states are

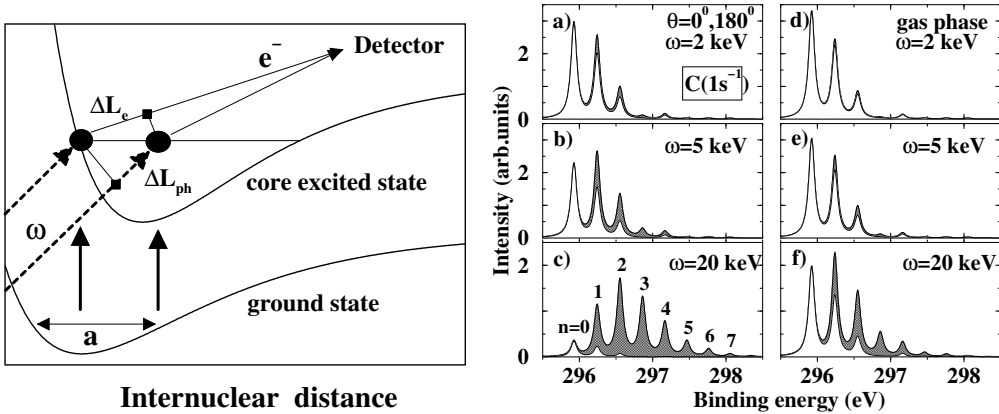


**Fig. 2.9:** (left) The GFC factors in X-ray photoionization.  $a$  is the size of the ground state wave packet. The phase difference depends on the spatial size of the wave packet, the observation angle as well as on the wavelength of the emitted particle.

**Fig. 2.10:** (right) Carbon K-level photoelectron spectra of CO for different photon energies.  $\mathbf{k} \uparrow \downarrow \mathbf{p}$ . Left panels (a,b,c) show the spectra for photoelectrons ejected parallel to the molecular axis. The case of randomly oriented molecules is shown in panels (d,e,f). The unshaded plots show the spectra calculated without phase factor  $\exp(i\alpha(\mathbf{k} - \mathbf{p}) \cdot \mathbf{R})$  (The spectra are normalized so that the low-energy peak has the same intensity in the two spectra). The shaded plots are calculated making use of the GFC factors. The adiabatic C 1s ionization potential (0 – 0 transition) is equal to 295.9 eV. See paper 11.

indistinguishable. The most interesting case is the destructive interference which can produce an *atomic hole* replacing the atomic peak. The atomic hole was first predicted in paper 2 of this thesis for a  $^4\Pi$  state – see Fig. 2.12. This state is effectively forbidden electronically and has therefore too small cross section to be observed. However, the atomic hole could be observed for another final state  $4\sigma^{-1}$  ( $^2\Sigma^+$ ) – see Fig. 2.13. The theoretical cross section for this state is shown in Figure 2.14 where we have taken into account also the direct photoionization cross section to reproduce the experimental ratio between the molecular background and atomic peak. Both figures show also the same state in the case of DCl, where the hydrogen atom has been replaced by its heavier isotope, deuterium. Both in practice and theory, the hole is gone for DCl. Since the HCl and DCl molecules have the same electronic structure and only the effective mass of the molecule is different, we can draw the conclusion that this effect depends on the dissociation

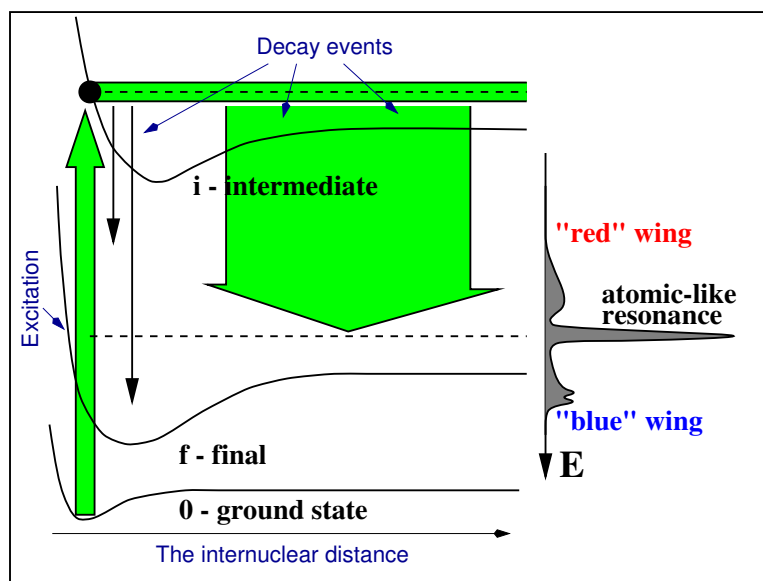


**Fig. 2.11:** The formation of molecular and atomic bands in RXS. The broad background is attributed to the decay in the molecular region while the atomic peak originates from the decay after dissociation.

speed. DCl dissociates slower than HCl and the atomic hole is not seen. Also, the duration of the RXS plays a crucial role in the competition between atomic peak (or hole) and molecular background. When the RXS duration is short (large detuning or lifetime broadening), the molecule has no time to dissociate and the atomic peak/hole is suppressed. The molecular band and atomic peak have qualitatively different dispersion laws. While the molecular background shifts up with increasing incident photon energy  $\omega$ , the position of the atomic peak is constant and does not depend on  $\omega$ . Furthermore, the resonance (Raman) narrowing below the core-excited lifetime width, which takes place for normal (here the molecular band) resonant X-ray scattering, does not hold for the dissociative atomic peaks. [16, 17, 15, 18]

The observation of the atomic hole is nontrivial since a set of conditions must be met. The core-excited state has to be dissociative and the core-excited state lifetime must be sufficiently long in order to observe atomic features in the spectrum. The bound final states have their molecular part shifted away from the atomic peak and it is unlikely to observe the atomic features with the incident

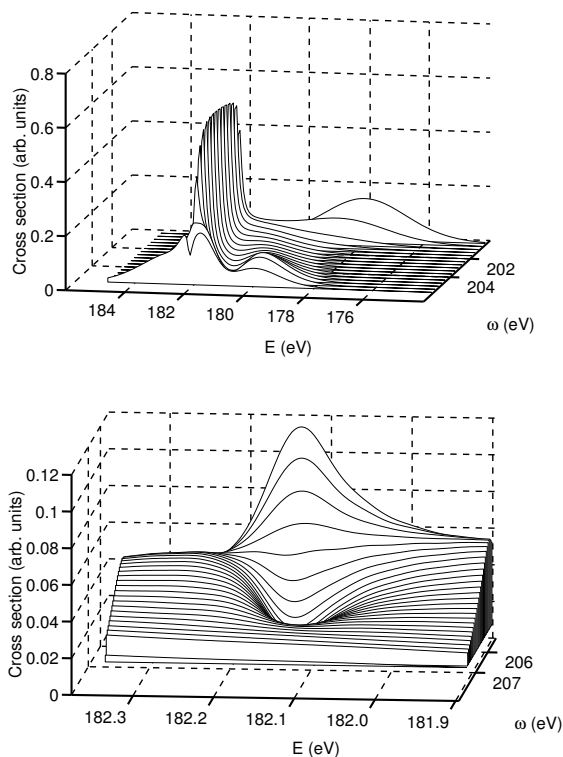


**Fig. 2.12:** The RXS cross section for the unbound  $4\Pi$  final state of HCl for different excitation energies. The RXS cross sections are normalized; the integral cross sections are the same for different excitation energies.  $\gamma = 0$  eV. The lower panel shows in more detail the region near the spectral hole. See paper 2.

photon energy detuned sufficiently to compensate for this shift due to small cross section. The dissociative final state should be separated in the energy space from the other states and be the only one having that particular atomic limit – the atomic peaks originating from other states would cover the hole otherwise. Also, the dissociation speed has some substantial significance, as can be understood from the DCl case.

## 2.6 HF – the merge of electronic and vibrational theories

A higher difficulty level in the RXS theory is to reproduce the complete RXS spectrum of the molecule which includes many, often overlapping, final states. One would like also to be able to include the direct channel with the weight computed by ab initio methods instead of estimating it from the experimental data.

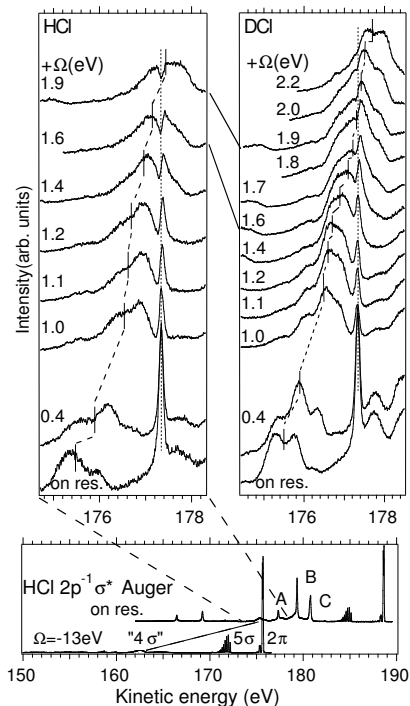


**Fig. 2.13:** The measured RXS cross section in the  $4\sigma^{-1}$  spectral region of HCl and DCl. See paper 3.

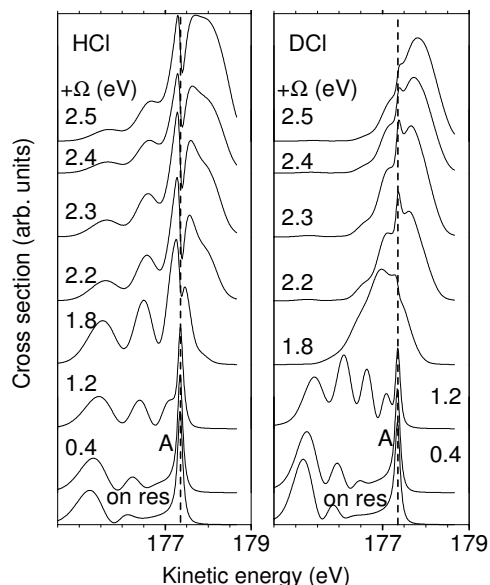


**Fig. 2.14:** Theoretical calculation of the observed HCl atomic hole. The calculation demonstrates the hole for HCl and the lack of it for DCl. See paper 3.

In order to compute such a spectrum, one needs to possess not only complete knowledge of all final states in the energy region of interest but also all the relevant transition moments. The calculation of the electronic transition moments where one of the states has one core electron removed is not quite routine. Calculations of the Auger decay rates involve description of free Auger electrons which requires special techniques [19, 20].

We investigated in paper 4 hydrogen fluoride, the lightest molecule in the group of halides. This molecule has a photoelectron spectrum where the spectator part contains strong atomic lines and a participator part with only molecular backgrounds – see Figure 2.15.

This molecule serves also as an exception from the participator-spectator classification: Frequently, the source and target orbitals of the electron decay occurring

in the scattering process can be easily identified. When the electron excited by the incident photon takes part in the decay process, the associated state is called a “participator”. When the excited electron remains in its place, the associated state is called a “spectator”. In the case of the core-excited HF molecule having an  $1\sigma^{-1}\sigma^*$  electronic configuration, the spectral feature associated with the final electronic state  $1\pi^{-1}$  is called a participator, and the spectral feature associated with  $1\pi^{-2}\sigma^*$  is a spectator. This naming convention is useful because these two types of states behave differently in the RXS process. The spectator states have negligible direct photoionization cross section because two electrons are displaced compared to the ground state configuration and photoionization is basically a one-electron process. They have, however, usually large resonant cross sections. The participator states, on the other hand, have usually non-vanishing direct photoionization cross sections. This clean distinction between these two classes disappears when two such configurations belonging to same symmetry cross. The electronic character of the state will change with the internuclear distance and so will the transition moments.

Presence of the strong direct ionization contribution may also lead to apparent quenching of the atomic peak – see the lowest HF participator states on Figure 2.16. While the purely resonant contribution associated with these states have evident atomic features, these features are small compared to the direct photoionization background.

The ab initio calculations (see Chapter 4 for more details) were not quite straightforward and included computation of potential curves for 9 final electronic states: 3 participators and 6 spectators. Also, the relevant transition moments were computed. Two of the spectators states  $1\pi^{-2}\sigma^*$  ( ${}^2\Sigma^-$ ) and  $1\pi^{-2}\sigma^*$  ( ${}^2\Delta$ ) could be discarded from further calculations because they lead to negligibly small Auger decay rates.

The X-ray excitation transition moments  $\hat{V}$ , the Auger decay transition moments  $\hat{Q}$  and the photoionization transition moments  $\hat{Z}$  were computed at a single point near the equilibrium geometry of the molecule. This choice is a good approximation because these transition moments associated with electronic configurations are controlled by the properties of the electronic wave function in the neighborhood of the fluorine atom and it was found numerically that the hydrogen-fluorine internuclear distance changes them to a very limited extent.

An important interplay of electron and nuclear degrees of freedom deserves a comment. One of the manifestations of the nuclear motion is the broadening of the spectral profile. Such a “vibrational broadening” results in the dynamical

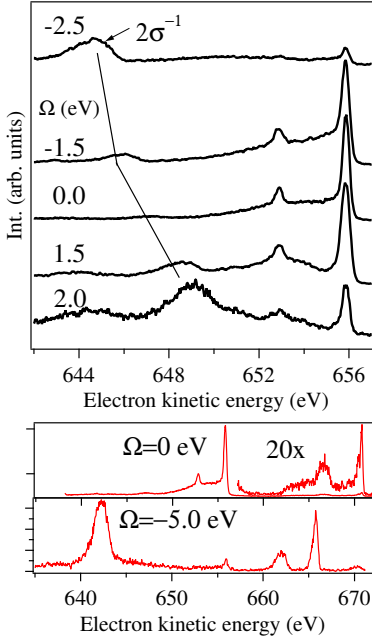


**Fig. 2.15:** The experimental HF spectrum. [21]

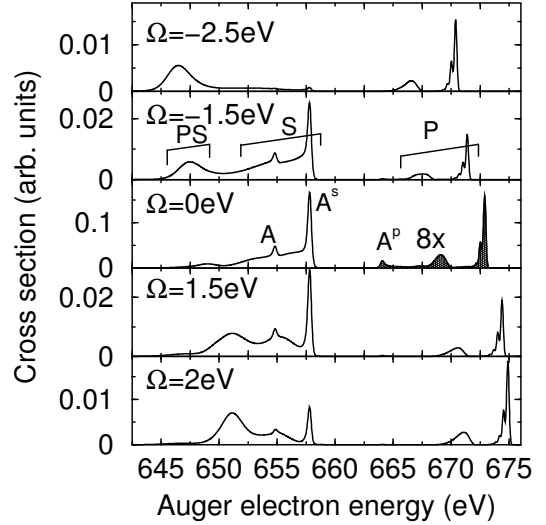


**Fig. 2.16:** Theoretical calculation of the RFXS spectrum of HF including resonant, direct and interference channels for 7 distinct final electronic states. The spectrum includes also lower participator bound states marked with P. See paper 5.

suppression of the resonant cross section due to an invariance of the total area of the resonant profile. This issue is treated in paper 5.

The calculations for the hydrogen fluoride molecule are slightly complicated by the avoided crossing between  $2\sigma^{-1}$  and  $3\sigma^{-2}\sigma^*$  states because the Auger decay rates associated with these two electronic configurations are diametrically different.  $2\sigma^{-1}$  is a participator configuration, with a large direct photoionization cross section and rather small resonance cross section while  $3\sigma^{-2}\sigma^*$  has the electronic configuration of a spectator state with a close to zero photoionization cross section and substantial resonance cross section. The adiabatic states defined by the linear combination of these configurations switch the transition moments at the avoided crossing giving rise to a strong  $R$ -dependence of the respective transition moments. This results in a sharp switching of the Auger decay rates after the avoided crossing point and changes qualitatively the role of the nuclear dynamics in the formation of the RPE spectra – see again paper 5 for details.

No, don't use `kill -9`. Don't bring out the combine harvester just to tidy up the flower pot.

## Chapter 3

# Wave packet methods

While electronic structure calculations generally give insight into the scattering process and allow for an estimation of the energy ranges, wave packet methods simulating the nuclear motion of the molecule induced in the scattering process are very helpful to understand the spectral shape of the cross section.

The spectral shape of the cross section can be investigated also by time-independent methods. These approaches, being computationally very efficient for bound states, become numerically expensive for dissociative states. Also, time-dependent wave packet methods are more natural for such a time-dependent process as X-ray scattering; the relation between the lifetime and the speed of vibrational or dissociative motion is an integral part of the theory.

In the wave packet language, the scattering process can be explained as follows: The internal energy of the molecule gained by the absorption of the incident X-ray photon is initially contained in the electronic degrees of freedom but this excited electronic structure induces a nuclear motion with the energy being transferred to vibrational or dissociative motion of the nuclei. Wave packet methods give therefore the most natural ways of describing the scattering process.

The name “wave packet method” embraces a broad range of approaches including also various semi-classical methods. We treat here only strictly quantum methods using a finite difference representation of the wave packet. The finite difference method represents a function by sampling its values at usually equidistant grid points. One can interpret it as an expansion of the wave function in basis functions which are localized on well determined points – see Fig. 3.1.

Wave packet techniques possess a strong competitive edge over time-independent approaches because they do not require explicit knowledge of the eigenfunc-

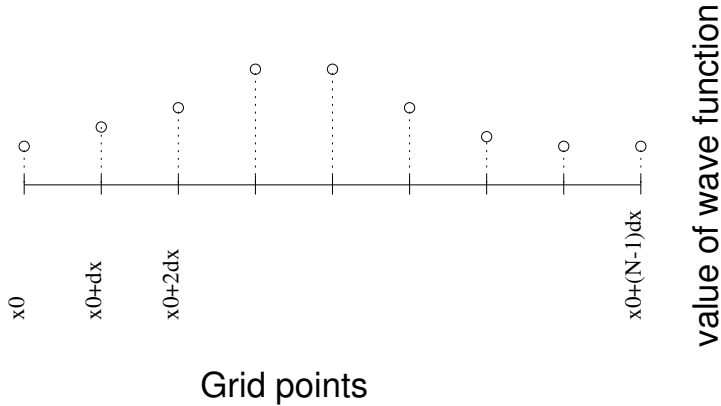


**Fig. 3.1:** The grid representation of the wave function. The function is represented by its values at a finite set of points. Usually, the points are equally spaced. The error introduced by this finite representation depends on the choice of spacing.

tions. Instead, only the time evolution operator has to be implemented. This property may not be decisive in the case of bound systems but it is a big win for dissociative states where a continuous energy spectrum is occupied; the time-independent methods would require to include all the relevant eigenfunctions which could be computationally challenging.

### 3.1 Absorption calculations

Wave packet methods which are used to compute absorption cross sections are natural starting points for more elaborate approaches used for scattering calculations. The cross section is computed as a Fourier transform of the autocorrelation function  $\sigma(t)$  of the ground state wave packet  $|0\rangle$  evolving on the potential surface of an excited state described by the Hamiltonian  $\hat{H}$ [22]

$$\sigma(\omega) \sim |V|^2 \int_{-\infty}^{\infty} \sigma(t) e^{i\omega t} dt, \quad \sigma(t) = \langle 0 | e^{-i\hat{H}t} | 0 \rangle \quad (3.1)$$

The autocorrelation function  $\sigma(t)$  is evaluated by computing the overlaps of the initial wave packet  $|0\rangle$  with this wave packet  $|\psi(t)\rangle = e^{-i\hat{H}t}|0\rangle$  at discrete time instances  $t_n$ .

### 3.2 Time-dependent techniques

Several definitions of the instantaneous probability or cross section circulate in the fields of laser and X-ray spectroscopies. Here we describe two time-dependent approaches used for evaluation of the RXS cross section. To understand the essence of these techniques we start from the kinetic equation for the final state population (see paper 7)

$$\frac{\partial}{\partial t}\rho_{ff}(t) + w_f(t) = P_f(t) \quad (3.2)$$

which shows that  $\rho_{ff}(t)$  changes due to the “income”,  $P_f(t)$ , and “outcome”,  $w_f(t)$ , contributions. The term

$$w_f(t) = 2\Gamma_f\rho_{ff}(t), \quad \rho_{ff}(t) = \langle \Psi_f(t) | \Psi_f(t) \rangle \quad (3.3)$$

describes the quenching of the final state population due to the decay in lower states. The “field” term

$$P_f(t) = 2 \operatorname{Im} \sum_c Q_{fc}(t)\rho_{cf}(t), \quad \rho_{cf}(t) = \langle \Psi(t) | \Psi_f(t) \rangle \quad (3.4)$$

changes the population of the final state due to the interaction with incident photon and emitted particles in the cascade  $|0\rangle \rightarrow |c\rangle \rightarrow |f\rangle$ . The off-diagonal element  $\rho_{fi}(t)$  of the density matrix describes the field induced polarization or coherence between final and core-excited states.

The existing schemes approach the problem from different sides and use  $P_f(t)$  or  $w_f(t)$  to compute the cross section. Let us present first the approach that evaluates the cross section from the population of the final state  $w_f(t)$ .

The evolution of wave packets of the ground, core-excited, and final states is described by the standard set of coupled Schrödinger equations

$$i|\dot{0}(t)\rangle = \hat{H}_0|0(t)\rangle \quad (3.5)$$

$$i|\dot{\Psi}(t)\rangle = (\hat{H}_c - i\Gamma)|\Psi(t)\rangle + \hat{V}(t)|0(t)\rangle \quad (3.6)$$

$$i|\dot{\Psi}_f(t)\rangle = (\hat{H}_f + E - i\Gamma_f)|\Psi_f(t)\rangle + \hat{Q}|\Psi(t)\rangle \quad (3.7)$$

where we took into consideration the fact that the perturbation of the ground state  $|0(t)\rangle$  introduced by the X-ray radiation field is negligible for presently available light sources. The core-excited state is pumped via the excitation operator  $\hat{V}(t)$  which is usually factored into three components

$$\hat{V}(t) = \mathcal{E}(t)(\mathbf{D} \cdot \mathbf{e}) e^{-i\omega t}$$

where  $\mathcal{E}(t)$  is the amplitude of the radiation pulse, and the latter exponential factor expresses the central frequency of the radiation field. It is instructive to remind that according to the uncertainty principle  $\mathcal{E}(t) \propto \delta(t)$  corresponds to broad band excitation, while  $\mathcal{E}(t) = \text{const}$  for a monochromatic incident light. The core-excited state is not energetically stable and decays with a total decay rate  $\Gamma$ . The final state is pumped through the partial decay rate  $\hat{Q}$  from the core-excited state. Having solved this set of equations, the instantaneous RXS probabilities for a given pair  $(\omega, E)$  can be obtained as the probability of the final state decay  $w_f(t)$  (3.3) or the probability  $P_f(t)$  or the transition between core-excited,  $\Psi(t)$ , and final,  $\Psi_f(t)$ , states. In the general case these probabilities differ from each other  $P_f(t) \neq w_f(t)$ . The discussion of this problem can be found in paper 7. However, as one sees from Eq. (3.2) both probabilities are the same

$$\lim_{t \rightarrow \infty} w_f(t) = P_f(\infty)$$

when the pulse duration is long compared to the lifetime of the final state  $\Gamma_f^{-1}$ , or when the radiation intensity does not depend on time, since  $\partial \rho_{ff}(t)/\partial t \rightarrow 0$  for  $t\Gamma_f \gg 1$ . The formalism based on an evaluation of  $P_f(t)$  is developed and used in ref. [8, 15, 23, 24, 25, 26, 27, 28, 29, 30, 21] and constitutes the foundation of our approach. Alternative techniques [31, 31, 18, 32, 33, 34, 35, 36, 37, 38] use  $w(t)$  to find the cross section. The transform of  $P_f(\infty)$  (3.4) in terms of the half-Fourier transform of the autocorrelation function  $\sigma(\omega, \tau)$  (2.4) can readily be carried out. For example the resonant part of  $\sigma(\omega, \tau)$  reads

$$\sigma_{res}(\omega, \tau) = \langle \Psi(0) | e^{-i(\hat{H}_f - E_0)\tau} | \Psi(0) \rangle. \quad (3.8)$$

To find the wave packet,  $|\Psi(0)\rangle$ , in the core-excited state we need to perform only one time integration (2.5).

Yet another scheme taking advantage of the fact that the core-excited and final potential surfaces are parallel in the dissociative region is derived in paper 2. The following equation defines the time propagator

$$\mathcal{U}(t, t_0) = \hat{T} \exp \left( -i \int_{t_0}^t e^{i\hat{H}_f\tau} \Delta U e^{-i\hat{H}_c\tau} \right) \quad (3.9)$$

$$\Delta V = \hat{Q}\hat{H}_c\hat{Q}^{-1} - \hat{H}_f \quad (3.10)$$

where  $\hat{T}$  is a time-ordering operator. This propagator can be used to compute the autocorrelation function of the wave packet  $|\psi(E)\rangle$  and – via a Fourier transform

– the cross section  $\sigma(\omega, E)$

$$|\psi(E)\rangle = \int_0^\infty e^{(iE-\Gamma)\tau} \mathcal{U}(\tau, 0) \hat{Q} \hat{D} |0\rangle d\tau \quad (3.11)$$

$$\sigma(\omega, E) = \frac{1}{\pi} \int_0^\infty \langle \psi(E) | e^{-i\hat{H}_f t} | \psi(E) \rangle e^{i(\omega-E-E_0)t} \mathcal{E}(t) dt \quad (3.12)$$

where  $\mathcal{E}(t)$  is, like above, the envelope of the X-ray pulse. In the dissociative region,  $\Delta V \rightarrow \omega_{cf}(\infty) = U_c(\infty) - U_f(\infty)$  and the time propagator simplifies to a number making the computation of  $|\psi(E)\rangle$  in Eq. (3.11) trivial. Generally, this method would though be more complex than the scheme described above.

*Is there any kind of text-mode visual editor on unix?*

If someone says, “vi”, someone else will inevitably reply, “emacs”.

If someone says, “emacs”, someone else will inevitably reply, “vi”.

If someone says, “ed”, everyone else tends to get quiet and assume that the person is either a Unix guru, an escaped mental patient, or both. Either way, they realize that they probably shouldn't argue the point further.

## Chapter 4

# Molecular electronic structure

The electronic structure of molecules is the most essential factor influencing the molecular interaction with light. For the energy and intensity range we work with, the light absorption is defined by the dipole transition moment of the molecule. The description of the interaction can be as simple as in Fig. 2.1.

Generally, gas molecules interact only with light of the frequency that corresponds to a transition between two discrete energies corresponding to different electronic wave functions. Actually, the transition is infinitely narrow only in the limit of infinite lifetime of the involved electronic states. The core-excited states we have been investigating have lifetimes of order 50 – 200 meV and the valence states have lifetimes usually two orders of magnitude longer.

Presently, valence excitation energies are computed routinely for small molecules at equilibrium geometries. This computation becomes more troublesome for larger molecules at dissociative geometries where it is not any longer possible to use closed shell singlet reference wave functions. Computation of core-hole states can often be even more difficult.

The transition probability between two electronic states determines the intensity of the transition. Again, this field is relatively well investigated for valence excitations of molecules at equilibrium geometries but the computations require state-of-the-art methodology when core-excited states are involved.

While single geometry calculations are sufficient to get much information about the localization of the spectrum in the energy space, more knowledge about the potential surfaces is necessary to be able to explain the spectral shape of the cross section. The shape is formed during the scattering process: The excited state has usually different equilibrium geometry – or is dissociative – and the electronically

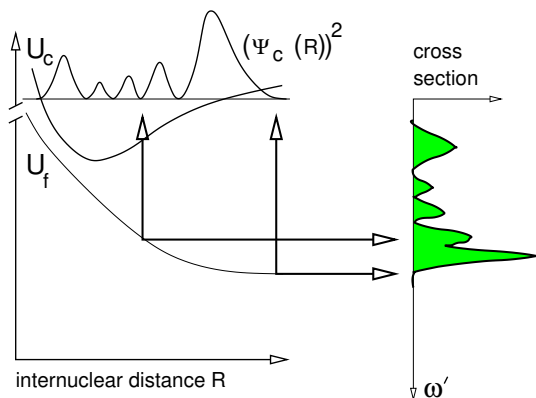


**Fig. 4.1:** The mapping of the core-excited wave packet  $\psi_c(R)$  on the final potential surface  $U_f$  [15].

excited molecule is also in a vibrationally excited state which can be mapped on to the cross section.

The mapping procedure – illustrated in Figure 4 – is actually a simple way to get an idea about the RXS process particularly when the final potential surface is dissociative or considerably displaced with respect to the core-excited potential surface. When this condition is fulfilled, the cross section will resemble the nodal structure of the core-excited vibrational wave function.

## 4.1 Potential surfaces

The potential surfaces needed for the wave packet studies of RXS can be obtained from spectroscopic data or ab initio electronic structure calculations. The spectroscopic data can be obtained from ordinary UV absorption experiments but is often limited to bound valence potentials.

Not all electronic structure methods are suitable for calculation of potential surfaces. The method must be size-extensible and handle open shells that emerge when bonds are broken on dissociation. We used the multi-configurational self-consistent field method (MCSCF). Whenever possible, we added active space second order perturbation (CASPT2) on top of it, or performed multi-reference configuration interaction (MR-CI) calculations. For core-excited states, we carried out a three step calculation for each point, obtaining first ground state reference orbitals, performing frozen core calculation forcing occupation of the core-hole orbital to 1, and finally relaxing the core hole in the field of the valence electrons.

Beside a balanced choice of the active space for the MCSCF method, the choice of basis set is also substantial. The excited states that are dealt with require large flexibility in the basis set and small basis sets describing well the ground state may not be sufficient any more.

#### 4.1.1 HF method

The Hartree-Fock method (also called self-consistent field (SCF) method) was developed to solve the electronic Schrödinger problem where the wave function  $\Phi$  describing  $N$  electrons in the system was constrained to be a single Slater determinant being a combination of single electron orbitals  $\phi_i(x)$

$$\Phi = \frac{1}{\sqrt{N!}} \begin{vmatrix} \phi_1(x_1) & \phi_2(x_1) & \cdots & \phi_N(x_1) \\ \phi_1(x_2) & \phi_2(x_2) & \cdots & \phi_N(x_2) \\ \vdots & \vdots & \vdots & \vdots \\ \phi_1(x_N) & \phi_2(x_N) & \cdots & \phi_N(x_N) \end{vmatrix} \quad (4.1)$$

The electron spin-orbitals  $\phi_i$  are formed as a linear combination of basis functions  $g_j(x)$

$$\phi_i(x) = \sum_j c_{ij} g_j(x) \quad (4.2)$$

The basis sets used in molecular calculations are usually generated from function sets attached to each atom in the molecule although one can also attach basis functions to bonds between atoms. The atom specific basis sets  $g_j(x)$  are often optimized in atomic calculations. The Hartree-Fock method can be reduced to minimalization of the molecular energy by optimization of the expansion coefficients  $c_{ij}$  by solving of the Hartree-Fock equation

$$\hat{f}(i)\phi_i = \epsilon_i\phi_i, \quad \hat{f}(i) = -\frac{1}{2}\nabla_i^2 - \sum_A \frac{Z_A}{r_{iA}} + v^{HF}(i) \quad (4.3)$$

All the electron-electron interaction is collected in the average potential in which the  $i$ th electron moves in. The only difficulty is caused by the fact that this average potential  $v^{HF}(i)$  depends on the solution of the Hartree-Fock equation. The solution has to be obtained in a self-consistent fashion, i.e, the Hartree-Fock equation is solved using trial orbitals to obtain the electron density needed in  $v^{HF}$ . The new orbitals generate a new electron density. The entire procedure is repeated until convergence is reached.

### 4.1.2 MCSCF method

The multiconfigurational self consistent field method, MCSCF, extends the single configuration Hartree-Fock method to represent multiconfigurational wave functions. The wave function in the MCSCF method is assumed to have the form:

$$|\Phi_{\text{MCSCF}}\rangle = \sum_R a_R |\Phi_R\rangle + \dots \quad (4.4)$$

where the summation is carried out over a selected set of determinants  $|\Phi\rangle$ .

The complete active space SCF method, CASSCF, is a variant of the general MCSCF method where the configurations used in the wave function optimizations are generated by dividing the orbital space in three parts: inactive, active and secondary. The configuration set includes all possible occupations of the orbitals in the active space; orbitals in the inactive space are always double-occupied and orbitals in secondary space are always empty.

### 4.1.3 Other high accuracy methods

The CASPT2 method is founded on a second order perturbation theory with CASSCF reference function. The second order perturbation methods make use of a partition of the Hamiltonian  $\hat{H}$  into an unperturbed Hamiltonian  $\hat{H}_0$  and the perturbation  $\hat{H}_1$ , and an expansion of the Hamiltonian's eigenvalues and eigenvectors  $E$  into a series:

$$\hat{H} = \hat{H}_0 + \lambda \hat{H}_1 \quad (4.5)$$

$$E = E_0 + \lambda E_1 + \lambda^2 E_2 + \dots \quad (4.6)$$

The Hamiltonian is partitioned so that the eigenfunctions and eigenvalues of  $\hat{H}_0$  can be easily obtained. One can insert this expansion into the Schrödinger equation, collect terms with same order of expansion parameter  $\lambda$  and obtain

$$\hat{H}_0 \Phi_0 = E_0 \Phi_0 \quad (4.7)$$

$$(\hat{H}_0 - E_0) \Phi_1 = (E_1 - \hat{H}_1) \Phi_0 \quad (4.8)$$

$$(\hat{H}_0 - E_0) \Phi_2 = (E_1 - \hat{H}_1) \Phi_1 + E_2 \Phi_0 \quad (4.9)$$

The 0th order energy  $E_0$  is the solution of the non-perturbed problem (4.7). The higher order corrections  $E_1$  and  $E_2$  can be evaluated from the perturbation matrix

elements. The CASPT2 method uses a CASSCF function as the zero order term in the perturbation expansion.

The multi-reference CI (MR-CI) methods approximates the wave function as an expansion in all single and double excited configurations with respect to a set of chosen reference configurations:

$$|\Phi\rangle = \sum_I (C_I |\Phi_I\rangle + \sum_{i,a} C_{I,ia} |\Phi_{I,ia}\rangle + \sum_{i,a,j,b} C_{Iiajb} |\Phi_{Iiajb}\rangle) \quad (4.10)$$

where  $I$  is a set of reference configurations  $\Phi_I$  (usually manually selected and read by the program from the calculation description file) and the other terms denote configurations where one or two occupied orbitals  $i, j$  have been replaced by one or two occupied or virtual orbitals  $a, b$ . The MR-CI method reduces to the ordinary single-double CI method in the case of a single reference configuration equal to the HF determinant. This method becomes very expensive with an increasing size of the molecule or basis set.

## 4.2 Computation of transition amplitudes

The computations of transition moments is an essential ingredient in addition to the calculations of the potential energy curves and solving the nuclear dynamics, in order to obtain the full picture of the spectrum formation. In principle, the information on the transition moments is needed i) when more than one state (transition) is to be described; ii) when the transition moments vary significantly with the geometry; iii) when there is more than one electronic process which contributes to the final state population. An example of the latter is the resonant photoemission process which comprises two main channels, the direct and the resonant channels. As already mentioned in the previous chapter both these channels are important even at resonant conditions, and sometimes the interference between them is also significant.

We analyze the RPE process using the following model. The molecule  $M$  in its ground state absorbs an X-ray photon with frequency  $\omega$  and is excited to the discrete resonant states. The Coulomb interaction results in autoionization of these discrete states to a set of final continuum states. The direct transition to such final states can also be considerable:

$$\omega + M \begin{array}{c} \nearrow \\ \Rightarrow \\ \searrow \end{array} \begin{array}{c} \sum_m M_{cm}^* \\ \\ \sum_{fm_f} M_{fm_f}^+ \end{array} + e^- \quad (4.11)$$

We are interested in three types of transition moments. The amplitudes of the direct photoionization  $\Phi_0 \rightarrow \Phi_f$  and resonant core excitation  $\Phi_0 \rightarrow \Phi_c$  are the matrix elements of the dipole moments

$$Z = \langle \Phi_f | \mathbf{D} \cdot \mathbf{e} | \Phi_0 \rangle, \quad V = \langle \Phi_c | \mathbf{D} \cdot \mathbf{e} | \Phi_0 \rangle. \quad (4.12)$$

The autoionization amplitude of the core-excited state

$$Q = \langle \Phi_f | \hat{H} | \Phi_c \rangle \quad (4.13)$$

is expressed in terms of the Coulomb integrals between one-electron states. For example, in a one-electron picture

$$Q \approx 2 \langle \phi_j \phi_v | \phi_{\beta\epsilon} \phi_c \rangle - \langle \phi_j \phi_v | \phi_c \phi_{\beta\epsilon} \rangle \quad (4.14)$$

for the ‘‘participator’’ channel ( $c \rightarrow \nu : \nu \rightarrow c; j \rightarrow \beta\epsilon$ ). The expression for spectator final states is similar.

The computations of transition moments involving core electrons are not so routine. One problem refers to the large relaxation of the wave functions between initial and final states. This makes the response (propagator) methods, that usually successfully describe spectra in the UV and optical regions, not easily applicable for core electron spectra. Another problem refers to the fact that core hole states (core electron excited states) are embedded in electronic continua. Formally this leads to problems with variational collapse, which often in practice though is a solvable problem. An effective algorithm to take care of the fact that orbitals are not orthogonal between initial and final states must then be applied.

When the transition involves the continuum electron directly (that is when a continuum orbital is contained in  $\Phi_f$ ), the handling of this continuum electron must be addressed in a special way. This is so for example for photoemission, which takes place from the ground state to the final core hole state with one electron in the continuum. This problem is especially relevant for molecules for which the potential in which the continuum electron moves is anisotropic, and for X-ray excitations, since the electron then moves with high energies. Special techniques have been devised to cope with this problem (Stieltjes imaging and K-matrix techniques, for example). For resonant photoemission (resonant Auger), the situation is more delicate in that it is a two-electron operator (actually the Hamiltonian  $\hat{H}$ ) which is responsible for the transition.

Paper 5 describes a technique based on so-called Stieltjes imaging which solves this problem in a way that is analogous to the direct photoionization case. This

paper could therefore address both the direct and the resonant photoionization channels, which indeed both were found significant for the RPE spectrum of HF, actually even at resonant conditions. The paper merges such calculations with the nuclear dynamics in order to obtain a complete picture how the RPE spectrum is formed when the core-excited state is dissociative. For instance, the role of the dynamics appears quite differently for the two channels. With this method RPE of general molecules can thus be addressed.

“Thinking implies disagreement; and disagreement implies non-conformity; and non-conformity implies heresy; and heresy implies disloyalty – so obviously thinking must be stopped.”

[Call to Greatness, 1954] – Adlai Stephenson

# Summary

This thesis collects the results obtained during my PhD studies that are connected to wave packet theory for resonant X-ray scattering.

The following main results closely related to experiment have been obtained:

1. We predicted a new spectral interference feature coined “atomic hole” (paper 2). This spectral feature was later experimentally confirmed (paper 3).
2. We explored the general conditions for formation of atomic peaks and atomic holes in dissociative resonant photoemission, and could attribute a dynamic suppression of atomic peaks to the significant role of direct photoemission even at resonant conditions (paper 5).
3. We predicted a Doppler effect for resonant X-ray scattering (paper 8), which subsequently was experimentally confirmed. For bound states the theory materialized to the introduction of generalized Frank-Condon factors (paper 9). The influence of such factors on vibrational fine structure in RXS scattering (paper 10) and in photoelectron spectroscopy (paper 11) was predicted and analyzed.
4. We studied the molecular geometry dependence of the transition moments (paper 12). This element of the theory was the key to explain the unusual spectrum flattening observed in the B-state spectra of  $N_2$  and for the breakdown of the spectator - participator classification in HF.
5. We developed wave packet theory of X-ray Raman scattering combining the electronic structure theory with nuclear dynamics. Both the direct and the resonant photoemission channels and also their interference were accounted for basing on first principle calculations.

6. We studied the relation between the temporal shape of the incident photon pulse and the measured RXS spectrum (paper 7).
7. The elements of the theory have been implemented in a numerical wave packet program described in detail in paper 6. All the numerical calculations of the spectral shape of the cross section, duration time, detuning effects, influence of the  $R$ -dependent transition moments, interference between resonant and direct photoionization channels, were performed with this program.

The Road goes ever on and on  
Down from the door where it began.  
Now far ahead the Road has gone,  
And I must follow, if I can.

[Lord of the Rings] – J.R.R. Tolkien

# Bibliography

- [1] T. Åberg and B. Crasemann. In G.Materlik, C.J.Sparks, and K.Fischer, editors, *Resonant Anomalous X-Ray Scattering. Theory and Applications*, page 431. North-Holland, Amsterdam, 1994.
- [2] F. Gel'mukhanov and H. Ågren. *Phys.Rep.*, 312:87, 1999.
- [3] G.B. Armen, H. Aksela, T. Åberg, and S. Aksela. *J.Phys B: At. Mol. Opt. Phys.*, 33:49, 2000.
- [4] M.N. Piancastelli. *J. Electron Spectrosc. Rel. Phen.*, 107:1, 2000.
- [5] S.L. Sorensen and S. Svensson. *J. Electron Spectrosc. Rel. Phen.*, 114-116:1, 2001.
- [6] J. Guo and J. Nordgren. *J. Electron Spectrosc. Rel. Phen.*, 110-111:105, 2000.
- [7] J.-E. Rubensson. *J. Electron Spectrosc. Rel. Phen.*, 110-111:135, 2000.
- [8] F.Kh. Gel'mukhanov, L.N. Mazalov, and A.V. Kondratenko. *Chem. Phys. Lett.*, 46:133, 1977.
- [9] F. Kaspar, W. Domcke, and L.S. Cederbaum. *Chem. Phys.*, 44:33, 1979.
- [10] A. Cesar, H. Ågren, and V. Carravetta. *Phys. Rev. A*, 40:187, 1989.
- [11] W. Eberhardt. In W. Eberhardt, editor, *Applications of Synchrotron Radiation. Springer Series in Surface Sciences, Vol.35*, page 203. Springer-Verlag, Berlin, Heidelberg, 1995.

- [12] F. Gel'mukhanov and L.N. Mazalov. *Opt.Spectrosk.***42**, 659 (1977) [*Opt.Spectrosc.(USSR)* **42**, 371 (1977)].
- [13] F. Gel'mukhanov and H. Ågren. *Phys. Rev. A*, 49:4378, 1994.
- [14] O. Björneholm, M. Bäessler, A. Ausmees, I. Hjelte, R. Feifel, H. Wang, C. Miron, M.N. Piancastelli, S. Svensson, S.L. Sorensen F. Gel'mukhanov, and H. Ågren. *Phys. Rev. Lett.*, 84:2826, 2000.
- [15] F. Gel'mukhanov and H. Ågren. *Phys. Rev. A*, 54:379, 1996.
- [16] E. Kukk, H. Aksela, S. Aksela, F. Gel'mukhanov, H. Ågren, and S. Svensson. *Phys. Rev. Lett.*, 76:3100, 1996.
- [17] F. Gel'mukhanov and H. Ågren. *Phys. Rev. A*, 54:3960, 1996.
- [18] E. Pahl, H.-D. Meyer, and L.S. Cederbaum. *Z. Phys. D*, 38:215, 1996.
- [19] B. Schimmelpfennig, B.M. Nestmann, and S.D. Peyerimhoff. *J. Electron Spectr.*, 74(3):173–186, 1995.
- [20] S. Bonhoff, K. Bonhoff, B. Schimmelpfennig, and B. Nestmann. *J. Phys. B.*, 30(12):2821–2834, 1997.
- [21] P. Sałek, V. Carravetta, F. Kh. Gel'mukhanov, H. Ågren, B. Schimmelpfennig, M.-N. Piancastelli, S.L. Sorensen, R. Feifel, I. Hjelte, M. Bäessler, S. Svensson, O. Björneholm, and A. Naves de Brito. . Submitted.
- [22] Eric J. Heller. *Acc. Chem. Res*, 14(12):368–375, 1981.
- [23] P. Sałek, F. Gel'mukhanov, and H. Ågren. *Phys. Rev. A*, 59:1147, 1999.
- [24] H. Ågren, F. Gel'mukhanov, and P. Sałek. *J. Jpn. Soc. Synchrotron Rad. Res.* **12**, 1 (1999).
- [25] P. Sałek, F. Gel'mukhanov, H. Ågren, O. Björneholm, and S. Svensson. *Phys. Rev. A*, 60:2786, 1999.
- [26] F. Gel'mukhanov, P. Sałek, A. Shalagin, and H. Ågren. *J. Chem. Phys.*, 112:5593, 2000.

- [27] M.N. Piancastelli, R.F. Fink, R. Feifel, M. Bäblier, S.L. Sorensen, C. Miron, H. Wang, I. Hjeltje, O. Björneholm, A. Ausmees, S. Svensson, P. Salek, F.Kh. Gel'mukhanov, and H. Ågren. *J.Phys B: At. Mol. Opt. Phys.*, 33:1819, 2000.
- [28] P. Salek, R.F. Fink, F.Kh. Gel'mukhanov, M.N. Piancastelli, R. Feifel, M. Bäblier, S.L. Sörensen, C. Miron, H. Wang, I. Hjeltje, O. Björneholm, A. Ausmees, S. Svensson, and H. Ågren. *Phys. Rev. A*, 62:062506, 2000.
- [29] R. Feifel, F. Burmeister, P. Salek, M.N. Piancastelli, M. Bäblier, S.L. Sörensen, C. Miron, H. Wang, I. Hjeltje, O. Björneholm, Naves de Brito, F.Kh. Gel'mukhanov, H. Ågren, and S. Svensson. *Phys. Rev. Lett.*, 85:3133, 2000.
- [30] P. Salek, F. Gel'mukhanov, T. Privalov, and H. Ågren. *Chem. Phys. Lett.*, 328:425, 2000.
- [31] L.S. Cederbaum and F. Tarantelli. *J. Chem. Phys.*, 98:9691, 1993.
- [32] E. Pahl, L.S. Cederbaum, H.-D. Meyer, and F. Tarantelli. *Phys. Rev. Lett.*, 80:1865, 1998.
- [33] E. Pahl, L.S. Cederbaum, and F. Tarantelli. *Phys. Rev. A*, 60:1070, 1999.
- [34] E. Pahl, J. Brand, L.S. Cederbaum, and F. Tarantelli. *Phys. Rev. A*, 60:1079, 1999.
- [35] Z. W. Gortel, R. Teshima, and D. Menzel. *Phys. Rev. A*, 58:1225, 1998.
- [36] Z. W. Gortel, R. Teshima, and D. Menzel. *Phys. Rev. A*, 60:2159, 1999.
- [37] Z. W. Gortel and D. Menzel. *Phys. Rev. A*, 58:3699, 1998.
- [38] C. Keller, M. Stichler, G. Comelli, F. Esch, S. Lizzit, Z.W. Gortel, W. Wurth, and D. Menzel. *Phys. Rev. B*, 60:16143, 1999.